SUPPORTING INFORMATION

Enlightening the photoactive Site of channelrhodopsin-2 by DNP-enhanced solid-state NMR spectroscopy

Johanna Becker-Baldus[a,b], Christian Bamann[c], Krishna Saxena[b,d],

Henrik Gustmann[e], Lynda J. Brown[f], Richard C. D. Brown[f], Christian Reiter[g],

Ernst Bamberg[c], Josef Wachtveitl[e], Harald Schwalbe[b,d]

and Clemens Glaubitz[a,b*]

a) Institute of Biophysical Chemistry, Goethe University Frankfurt, Max-von-Laue-Str. 9, 60438 Frankfurt, Germany.

b) Centre for Biomolecular Magnetic Resonance, Goethe University Frankfurt, Max-von-Laue-Str. 9, 60438 Frankfurt, Germany.

c) Max-Planck-Institute of Biophysics, Max-von-Laue-Str. 3, 60438 Frankfurt, Germany.

d) Institute of Organic Chemistry and Chemical Biology, Goethe University Frankfurt, Max-von-Laue-Str. 7, 60438 Frankfurt, Germany.

e) Institute of Physical and Theoretical Chemistry, Goethe University Frankfurt, Max-von-Laue-Str. 7, 60438 Frankfurt, Germany.

f) Department of Chemistry, University of Southampton, Southampton SO17 1BJ, United Kingdom.

g) Bruker Biospin GmbH, Silberstreifen 4, 76287 Rheinstetten, Germany.

(*) Correspondence: Institute of Biophysical Chemistry

Goethe University Frankfurt

Max-von-Laue-Str. 9

60438 Frankfurt

Germany

Tel/Fax: 0049-69-798-29927/29

Email: glaubitz@em.uni-frankfurt.de

(A) Material and Methods

Preparing non-labeled and ^{15}N-labeled ChR2

Non-labeled ChR2 (amino acids 1 to 315) was purified as described before from membranes prepared from *P. pastoris* cultures grown in complex medium without retinal (1).

So far, isotope enriched ChR2 has not been produced. Therefore, a new approach had to be established to express recombinant ^{15}N-labeled ChR2 in *P. pastoris*. Due to the repeated observation that the recombinant production of this protein in minimal medium with stable isotopes led to growth arrest of *P. pastoris* we developed a specific expression protocol for this purpose. While recombinant ChRs and chimera have been generated in cells from several eukaryotic species like insect cells (2) that require expensive rich media for isotopic labeling this is the first report of stable-isotope ^{15}N labeled ChR2 expression. For uniformly ^{15}N labeled ChR2 production, cells were precultured in buffered minimal glycerol medium BMG^{S} supplemented with the Trace metal solution and a vitamin solution (10 µM thiamine, 10 µM NAD, 10 µM vitamin $_{B12}$ (3)): 1.34% yeast nitrogen base without amino acid, 0.00004% biotin, 1% glycerol, 0.1 M phosphate buffer at pH 6, 20 mL culture in a 100 mL baffled flask) containing 10 g/L $(^{14}NH_4)_2SO_4$ as the sole nitrogen source at 30 °C, 200 rpm (Infors multitron shaker, shaking hub 50 mm), until an OD_{600} of 5-10 was reached. Adaptation of the cells from ^{14}N to $(^{15}NH_4)_2SO_4$ (Eurisotop, Saarbrücken, Germany) as nitrogen source was performed by diluting (1:20) the cells to OD_{600} of 0.3 by addition of fresh ^{15}N BMG medium. This culture was grown to OD_{600} of 7-12 at 30 ^{o}C and 200 rpm (50 ml in in 1-L baffled flask). Cells were subsequently diluted to OD_{600} of 0.3 by addition of fresh ^{15}N BMG medium (final volume 1L in a 5 L baffled flask), incubated at 30 °C, 150 rpm until an OD_{600} of 12-14 was reached and harvested by centrifugation at 3000 *g* for 10 min at room temperature. Target protein expression was induced by carefully resuspending the pellet in 12 L of induction medium BMM^{S} (BMG^{S} with glycerol replaced by 5 mL/L methanol) with a starting OD_{600} of 2-3 in 5-L baffled flasks. Cultures were incubated at 30°C with shaking (140 RPM) for 5 -7 days and methanol (5 ml MeOH plus 50 ml water) was added every 24 hours to a final concentration of 0.5% provided that the cultures did grow. Finally, cells were pelleted at 3000 *g* for 10 min and subsequently used for membrane preparation (Fig. S6).

ChR2 reconstituted with 14-15-$^{13}C_2$-all-trans retinal

For reconstitution with the isotope labeled or unlabeled retinal compounds, we incubated the crude membrane preparation with 5 µM retinal for 2 h on ice before starting the solubilization with 1 % [m/v] β-decyl-maltoside (DM). 14,15-$^{13}C_2$-retinal was synthesized as described before (4). The final samples were concentrated in 20 mM Hepes, pH 7.4, 100 mM NaCl, 0.15% DM.

Reconstitution in proteoliposomes

ChR2 was reconstituted into proteoliposomes prepared from a mixture of POPC:POPG:cholesterol [8:1:1, m/m/m]. The lipids were dissolved in 2% cholate before adding the protein to a final lipid:protein ratio of 3:1 [m/m]. The detergent was extracted by several addition of BioBeads over the time course of 42 h at 4 °C.

Samples for DNP-enhanced MAS NMR

14,15-$^{13}C_2$-retinal-^{15}N-ChR2 proteoliposoms, containing 1.8 mg protein, where pelleted by ultracentrifugation for an hour. 88 µl of DNP buffer (20 mM AMUPOL (5), Fig 1), 30 v/v% d-8-Glycerol, 60 v/v% D_2O, 10 v/v% H_2O) was carefully layered above the pellet and incubated over night. Then the supernatant was removed and the sample was divided into two parts. The larger fraction was packed into a standard 3.2 mm ZrO_2 rotor and the smaller one into a 3.2 mm sapphire rotor. The sample in the sapphire rotor was then spun in an NMR probe with a few kHz at room temperature to distribute the sample on the inner surface of the rotor to optimize light penetration into the sample. From the relative signal intensities it was judged that sample in the sapphire rotor contained 20% of the sample packed in the ZrO_2 rotor, which correspond to 0.3 mg and 1.5 mg of protein, respectively.

DNP enhanced MAS NMR and illumination

DNP enhanced MAS NMR spectra were recorded on a Bruker 400 DNP system consisting of a 400 MHz WB Avance II NMR spectrometer, a 263 GHz Gyrotron as microwave source and a 3.2mm HCN Cryo MAS probe. All experiments were conducted with 8 kHz MAS and the microwave power at the probe was 10.5 W. During DNP experiments the temperature was kept at around 110 K. Referencing for ^{13}C and ^{15}N was done indirectly to DSS using the low field ^{13}C-signal of adamantane at 40.49 ppm. For all experiments 100 kHz decoupling using SPINAL-64 (6) was applied during acquisition.

^{13}C and ^{15}N CP experiments were recorded using ramped CP from ^{1}H to ^{13}C during 0.8 ms. The ^{15}N-detected double CP experiment was performed using a 6 ms specific CP (7) step. ^{13}C-double quantum filter experiments (DQF-experiments) were obtained using the POST-C7 (8) sequence for double quantum excitation and reconversion. By varying the number of excitation and reconversion blocks the signal intensity in the double quantum filtered spectra could be optimized or the full double quantum build-up curve was recorded. Using the isolated C15 signal, the double quantum efficiency was estimated to be 55%. For HCCH torsional angle measurements a double quantum heteronuclear local field experiment (9) was applied (HCCH-experiment). In the experiment POST-C7 during two rotor periods was used for double quantum excitation and reconversion, PMLG-9 (10) at 106.2 kHz was used for homonuclear ^{1}H decoupling and ^{1}H CW irradiation at 106.2 kHz was used during the constant time periods. All experiments were recorded with a recycle delay of 3 s. Spectra in (Fig. 2b)

were recorded with 128 scans except for CP at RT for which 106496 scans were required. For each data point in (Fig. 2c) and (Fig. 2d), spectra with 768 and 2048 scans were recorded, respectively. Spectra in Fig. 3 were recorded with 128 and 24576 scans, for the CP and DCP spectra, respectively. Number of scans in Fig. 4 were 8192 (^{13}C-DQF, dark and illuminated), 16385 (^{15}N DCP, dark) and 24576 (^{15}N DCP, illuminated). All spectra in Fig. 5 were recorded with 8192 scans. Illumination was done with a cold light lamp (Zeiss, KL 1500) using a blue filter (width 400-480 nm, maximal intensity 460 nm). Two methods of illumination were tested. Illumination outside of the NMR magnet was carried out by fixing the NMR rotor at its cap and subjecting it to a stream of cold nitrogen gas. Illumination was then switched on for 10 min, then the lamp was positioned on the opposite side of the rotor and another 10 min illumination was applied. Then the lamp was switched off and the rotor was kept close to liquid nitrogen temperatures during transport to the magnet. Then the cold rotor was inserted into the precooled NMR probe (100 K).

Later the probe was equipped with a light guide illuminating the spinning rotor from the walls through the openings of the coil. Illumination was done for 10-30 min. Both illumination protocols give indistinguishable results whereas the latter method is easier to handle, allows better temperature control but does not enable for rapid freezing, as the whole probe has to be cooled down.

For thermal relaxation experiments, as described by Mak-Jurkauskas et al. (11), the temperature of the spinning sample was changed after illumination at 110 K by changing the temperature of the bearing, drive and variable temperature-gas flows. Once the desired temperature had been reached, the sample was kept there for 10 min and then cooled down to around 110 K for performing the DNP-enhanced MAS NMR experiments.

For experiments with illumination at higher temperatures (thermal trapping) the rotor was either illuminated at the desired temperature and then quickly frozen and inserted into the cold probe or the sample was spun in the MAS probe at around 8 kHz and illuminated at the chosen temperature. Then the spinning sample was cooled down to 110 K for recording of the DNP-enhanced MAS NMR spectra.

Ambient temperature experiments

14,15-$^{13}C_2$-retinal-^{15}N-ChR2 proteoliposomes were pelleted by ultracentrifugation for one hour. The obtained wet pellet was transferred to a 3.2 mm MAS rotor. ^{13}C CP spectra were recorded on a Bruker 850MHz WB Avance III NMR spectrometer equipped with a Bruker 3.2 mm HCN MAS probe. The nominal temperature set was 270 K, the temperature inside the rotor is estimated to be 10-20 K higher. ^{13}C polarization was generated by a ramped CP from ^{1}H to ^{13}C during 1 ms and 100 kHz

decoupling using SPINAL-64 (6) was employed during acquisition. The recycle delay was 3 s. Referencing was done indirectly to DSS using the low-field ^{13}C-signal of adamantane at 40.49 ppm. The spectra at an MAS rate of 13 kHz and 16.6 kHz were recorded with 106496 transients each.

Data Analysis and Simulations

All spectra were analyzed and if appropriate integrated using TOPSPIN 2.1 (Bruker). If appropriate the signals of the C14 and C15 atoms where added and analyzed together. Deconvolution was applied prior to integration for overlapped signals.

Fitting of DQ build-up data: DQ build-up data were simulated with SIMPSON using an input file adapted from an example by Bak 2000 et al. (12). CSA parameters where taken from Smith et al. (13). DQ build-up curves where calculated with varying ^{13}C-^{13}C dipolar couplings. The obtained curves were fitted to the experimental data by multiplying them with a mono exponential decay function and the ^{13}C-^{13}C dipolar couplings was then obtained from the best fitting curve.

The correct performance of the DQ build-up experiments was validated using 2,3-$^{13}C_2$-disodium fumarate (Sigma Aldrich). Data were recorded at 100 K using the same parameters as for ChR2 but without microwave irradiation and with a recycle delay of 50 s. The spin system used for the SIMPSON calculation was taken from Carravetta et al., who used 2,3-$^{13}C_2$-diammonium fumarate and determined a bond length of 1.345 ± 0.013 Å (14). Experimental data and simulations are shown in Fig. S7. The obtained distance of 1.37 Å compares well within the experimental error (±0.025Å) with the previously reported NMR and X-ray data (14, 15). Small deviations are caused by the temperature difference (100 K vs. RT), the usage of a slightly different compound (2,3-$^{13}C_2$-disodium fumarate vs. 2,3-$^{13}C_2$-diammonium fumarate), which could result in altered CSA tensor orientations and different DQ excitation schemes. It should be noted that the exact distance determination depends on the knowledge of the Euler angles of the involved CSA and dipolar tensors. As these angles are unknown for our retinal compound a systematic error remains. In addition, distances determined by this method using solid state NMR are generally found to be slightly larger compared to what is observed by X-ray crystallography (14). It can be concluded that the absolute distances determined contain a larger uncertainty than when comparing distance differences using the same method as done here. However, the deviations are estimated to be within the numerical error.

Fitting of HCCH torsional angle data: The data was simulated with SIMPSON and the input file was adapted from Mao et al (16). The spin system was calculated based on a ^{1}H-^{13}C distance of 1.13 Å (17, 18), a ^{13}C-^{13}C distance as obtained from the DQ build-up data of 1.51 Å and a CHH angle of 115° (17, 19). The CH dipolar coupling was then multiplied with the PMLG scaling factor of 0.57 as the PMLG part was not explicitly simulated. The obtained curves were then fitted to the experimental data by

multiplying them with a mono exponential decay function and the ^{1}H-^{13}C-^{13}C-^{1}H torsional angles was then obtained from the best fitting curve.

Validation of the HCCH experiment was done using 2,3-$^{13}C_2$-disodium fumarate (Sigma Aldrich). The experiment was recorded at 100 K using the same parameters as for the ChR2 samples but without microwave. The obtained angle of 180° (Fig. S8) agrees perfectly with the dihedral angle in the fumarate anion and with previous experimental data (20-22). The spin system for the calculations was based on standard values as used by Feng et al. (23).

UV/vis Spectroscopy under cryogenic conditions

UV/vis-difference spectra were recorded with the help of a fiber-optic spectrometer (Ocean Optics, USB2000+). Probe light was provided by a balanced deuterium halogen-source (Ocean Optics, DH-2000-BAL). The sample temperature was controlled with the help of a liquid nitrogen cooled cryostat (Oxford Instruments, OptistatDN). For illumination a cold light lamp (Zeiss, KL 1500) with a blue filter (width 400-480 nm, maximal intensity 460 nm) was coupled into the cryostat and the sample was irradiated for 10-20 minutes at the target temperature.

The sample was prepared in a shortened 1x10 mm quartz cuvette (Hellma, 100-QS). For cryoprotection and reduction of light scattering 60%vol glycerol (Sigma-Aldrich, spectrophotometric grade) was added to the proteoliposomes.

All spectra where recorded at 150 K and subtracted from a dark spectrum recorded before one of the following illumination protocols: a) The sample was illuminated for 20 min at 150 K (Fig. 4). b) A thermal relaxation experiment where the sample illuminated as in a) and then heated up to 245 K. The sample was kept at this temperature for 10 min. Then it was again cooled to 150 K for recording the UV/vis spectrum (Fig. S4). c) The sample was heated to 245 K and illuminated for 10 min. Finally; it was cooled without illumination to 150 K for recording the UV/vis spectrum (Fig. S4).

The spectra were measured with an integration time of 100 ms and 400 scans were averaged. As reference for the absorption spectra the empty cryostat was used. To correct the influence of scattered light, all spectra were baseline corrected (OriginLab, OriginPro 9.0.0G). After subtraction of the dark spectrum, the resulting difference spectra were smoothed with the help of a moving average over 5 points.

(B) C14 and C15 Chemical Shifts of ChR2, Bacteriorhodopsin and Proteorhodopsin

Table S1: Chemical shifts and absorption maxima of different retinal proteins. All chemical shifts were determined at around 100 K under DNP conditions if not otherwise mentioned.

	C14 [ppm]	**C15** [ppm]	**^{15}N pSB** [ppm]	**λ_{max}** [nm]	**Conformation**
ChR2	126.3	166.5	196.5	470	all-*trans*, 15-*anti*
Bacteriorhodopsin light adapted (11, 24)	123.1	160.0	165.2	568	all-*trans*, 15-*anti*
Bacteriorhodopsin, dark adapted (11, 24)	123.1 111.0	160.0 163.2	165.2 173.5	568 555	all-*trans*, 15-*anti* 13-*cis*, 15-*syn*
Proteorhodopsin (4)	120.2	161.1	182.0	520	all-*trans*, 15-*anti*
Proteorhodopsin A178R (4)	122.1 110.7	160.7 165.6	182.1 -	533	all-*trans*, 15-*anti* 13-*cis*, 15-*syn*

(C) Comparison to previously reported data from vibrational spectroscopy

Resonance Raman experiments are non-invasive and should give reliable information on the retinal chromophore. However, assignment of the vibrational bands is very challenging and cannot easily be transferred between different systems. In dark adapted Bacteriorhodopsin a C14H out-of-plane wagging vibration at 800 cm^{-1} is detected, which vanishes after light adaption and is a marker band for the 13-*cis* conformer (25). However, this marker band is covered in resonance Raman spectra of ChR2 by lipid or detergent signals. Thus the ChR2 finger print region of the resonance Raman spectrum was analyzed in analogy to other retinal proteins (26). Assignment of the vibrational bands in the finger print regions is not straightforward and usually needs a rigorous assignment based on differently isotope labeled retinals as done for bacteriorhodopsin (27). To our knowledge, such an assignment is missing for ChR2 and therefore the interpretation of the resonance Raman data remains ambiguous. In contrast solid state MAS NMR can easily distinguish between the numbers of conformers present in the functional protein by simply counting the NMR signals.

The data in Fig. S4. show that the C14-C15 bond stretching and twisting is conserved in the trapped states within the experimental error limits. At first glance, some changes in the K- and M-like states might be expected. So far, no comparable K-state NMR data have been reported for other retinal proteins such as bacteriorhodopsin or proteorhodopsin. Raman data however suggested for bacteriorhodopsin a non-quantified bond twisting based on the occurrence of a “hydrogen-out-of-plane (HOOP)”-band assigned to the proton bound to C15 (28, 29). This band disappears already in the L-state. On the other hand, solid-state NMR experiments on bacteriorhodopsin have shown, that the bond is already twisted in the ground state and its out-of-plane orientation increases in the M-state (22). In case of ChR2, HOOP bands (986 cm^{-1}) have been reported, which were assigned and

interpreted based on bacteriorhodopsin data (30). It is currently unresolved how these vibrational bands relate to the H-C14-C15-H out-of-plane twist directly observed by solid-state NMR. Schiff base deprotonation in the M-state should also affect the C14-C15 bond. Indeed, solid-state NMR has shown for bacteriorhodopsin that the H-C14-C15-H torsion angle changes from 164° to 150° (22). In our case however, no data for the ChR2 M-like state could be recorded, as this state could not be trapped.

(D) Supporting Data

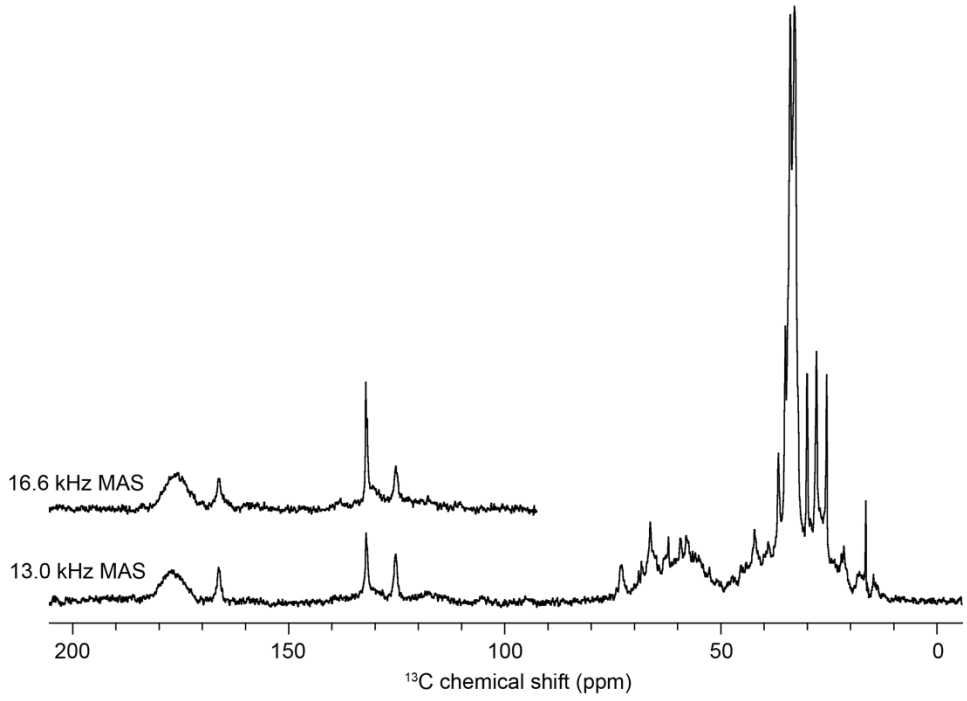

Fig. S1: Room temperature control spectra of 14,15-$^{13}C_2$-retinal-ChR2 recorded on a 850 MHz spectrometer using 13.0 kHz and 16.6 kHz MAS, respectively. All small signals around 110 ppm originate from spinning side bands and no 13-*cis*,15-*syn* chromophore conformation is detectable. The retinal resonances C14 (125.2 ppm) and C15 (166.2 ppm) are very similar to those recorded under DNP conditions. The small differences stem from temperature effects. The experiment confirms that the retinal within ChR2 exists in purely all-*trans*,15-*anti* conformation. Some of the signals detected in the DNP-spectra in Fig. 2 between 130 and 150 ppm are not observed here at room temperature due the higher lipid dynamics resulting in much reduced spinning side band signals and due to aromatic side chain dynamics which either lead to line broadening due to intermediate motion and reduced cross polarization efficiencies.

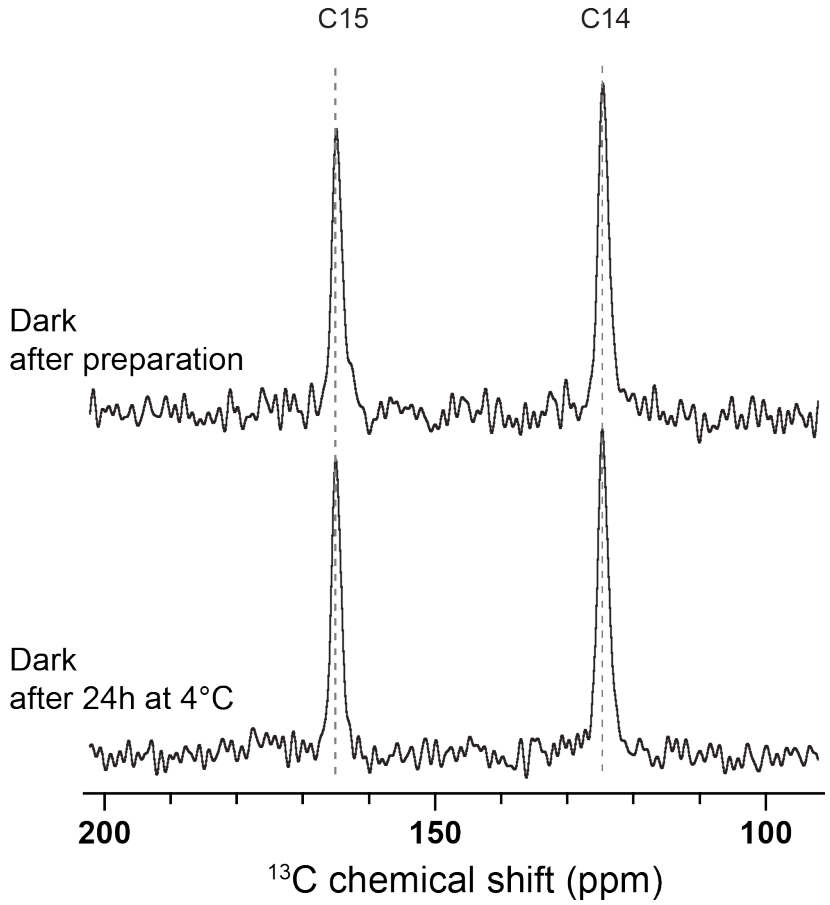

Fig. S2: DNP enhanced ^{13}C DQF spectra of ChR2 recorded immediately after preparation and again after storage at 4°C for 24 h. Identical signals are observed in both spectra showing no dark adaption.

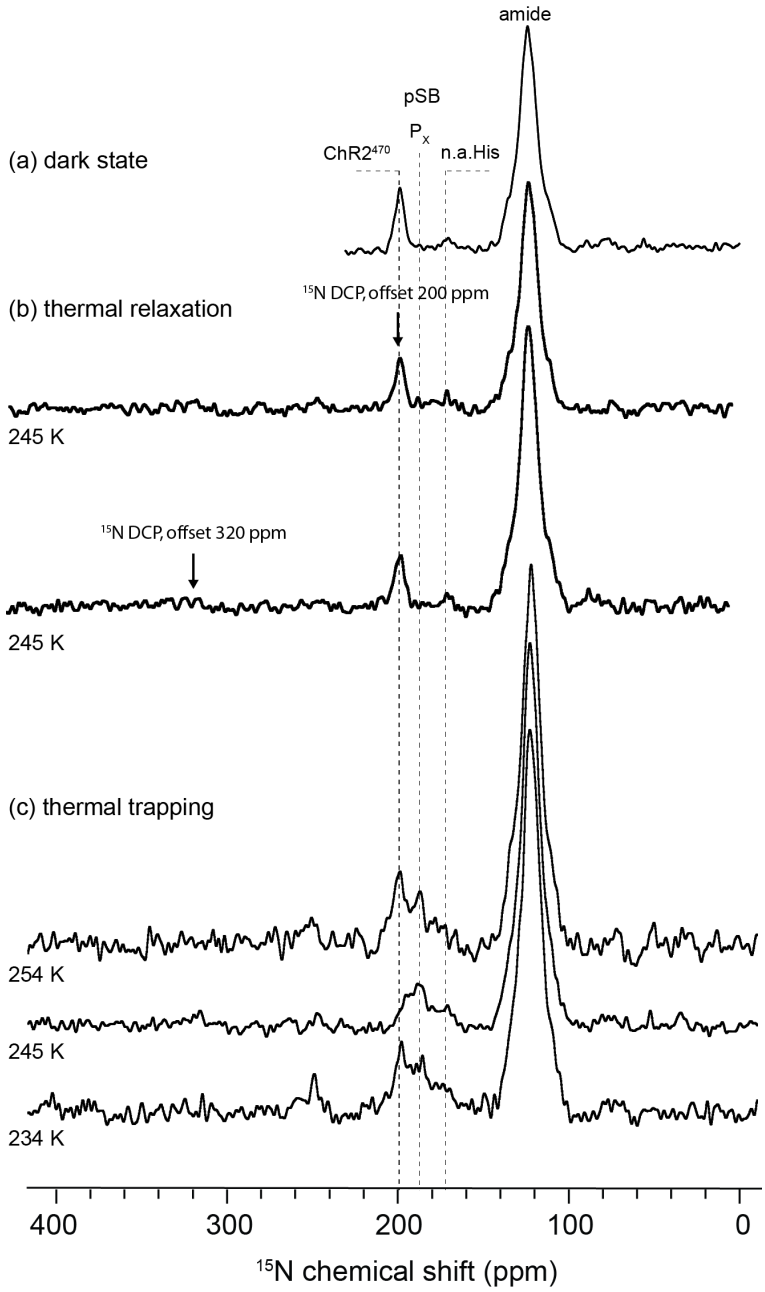

Fig. S3: ^{15}N-DCP filtered spectra of ChR2 in different states. **(a)** Ground state ChR2^{470} with a pSB chemical shift at 196.5 ppm. **(b)** Spectra obtained using the thermal relaxation protocol (see Fig. 5a). A resonance similar to ChR2^{470} is detected. In order to probe whether deprotonated Schiff base species would occur around 300 ppm, a second spectrum with shifted spectrometer offset was recorded. No indication for a deprotonated species was found. **(c)** Spectra obtained using the thermal trapping protocol (see Fig. 5b). The ground state signal at 196.5 ppm is depleted and a new signal occurs at 185 ppm, which is not visible under thermal relaxation conditions and which is therefore assigned to the P_x state. No peak could be identified for the P_4^{480} state, which might be due to severe line broadening. This could be caused by an ensemble of many different interactions the Schiff base might be involved in during this long-lived state.

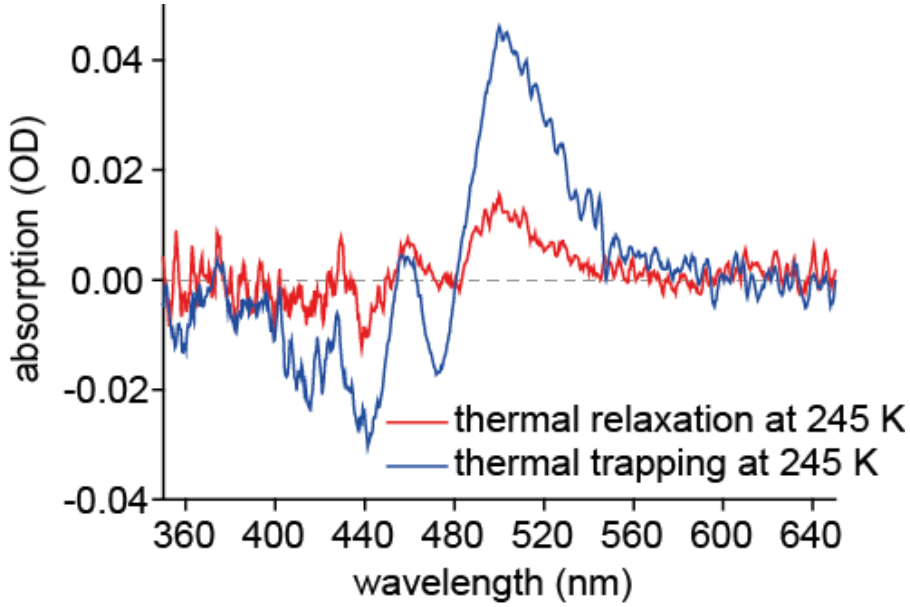

Fig. S4: Optical difference absorption spectra of ChR2 samples similar to those used for DNP-enhanced MAS-NMR acquired after subjecting the samples to the thermal relaxation and the thermal trapping protocols at 245 K. The difference spectrum of ground state and the 245 K thermally relaxed state shows some ground state bleaching and increase of a red shifted intermediate. This is in good agreement with the corresponding NMR spectra, which contain a large ground state signal for ^{13}C14 and a smaller signal for P_4^{480}. In contrast, the optical difference spectrum of ground state and the 245 K thermally trapped state shows significant differences. The large ground state bleaching agrees well with the ground state depopulation observed by solid state NMR spectroscopy. In addition, a pronounced signal maximum is observed at 500 nm. Thus, the optical data confirms that the thermal relaxation and the thermal trapping protocols at 245 K result in different population of photo intermediates. These data confirm that the thermal relaxation and the thermal trapping protocols at 245 K result in different population of photo intermediates.

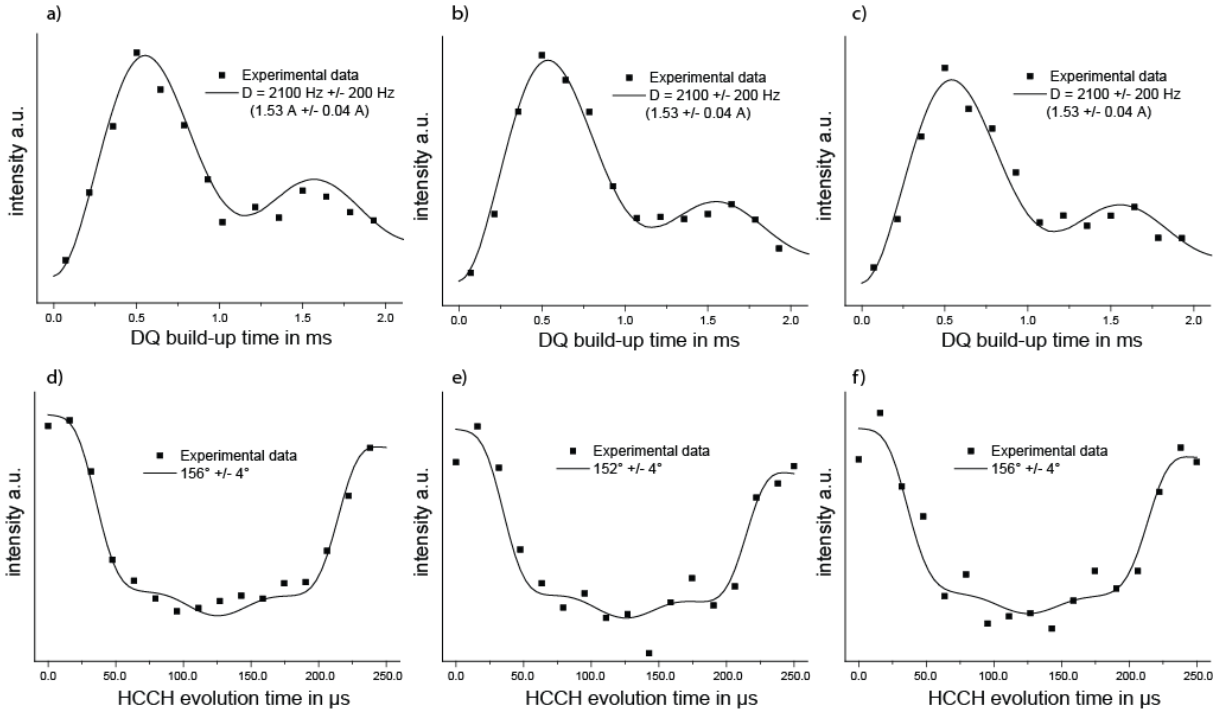

Fig. S5: **a-c)** ^{13}C14-^{13}C15 double quantum build-up curves and **d-f)** H^{13}C14-H^{13}C15 dipolar evolution curves recorded for differently trapped ChR2 states: **a+d)** P_1^{500}, K-like state, from the deconvoluted ^{13}C14 signal as seen in Fig. 4b) **b+e)** P_4^{480}, from the deconvoluted ^{13}C14 signal as seen at 245 K in Fig. 5a) **c+f)** P_x, from the deconvoluted ^{13}C14 signal as seen at 245 K with blue light in Fig. 5b). Our data show that the observed stretching and twisting of the C14-C15 bond remains unchanged in our trapped states within the experimental error. Further discussions are found in the main text in in section (C) of the supporting information.

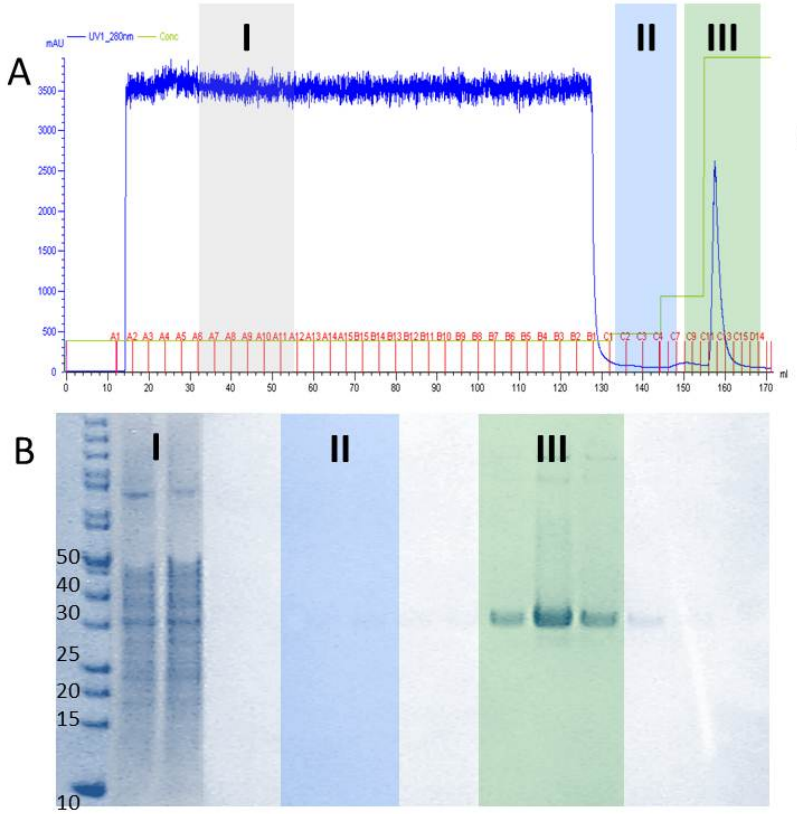

Fig. S6: Purification of ^{15}N-labeled ChR2. A) Elution profile of IMAC (Immobilized metal ion affinity chromatography). B) SDS-PAGE of IMAC elution fractions with a molecular weight reference marker (kDa) on the left.

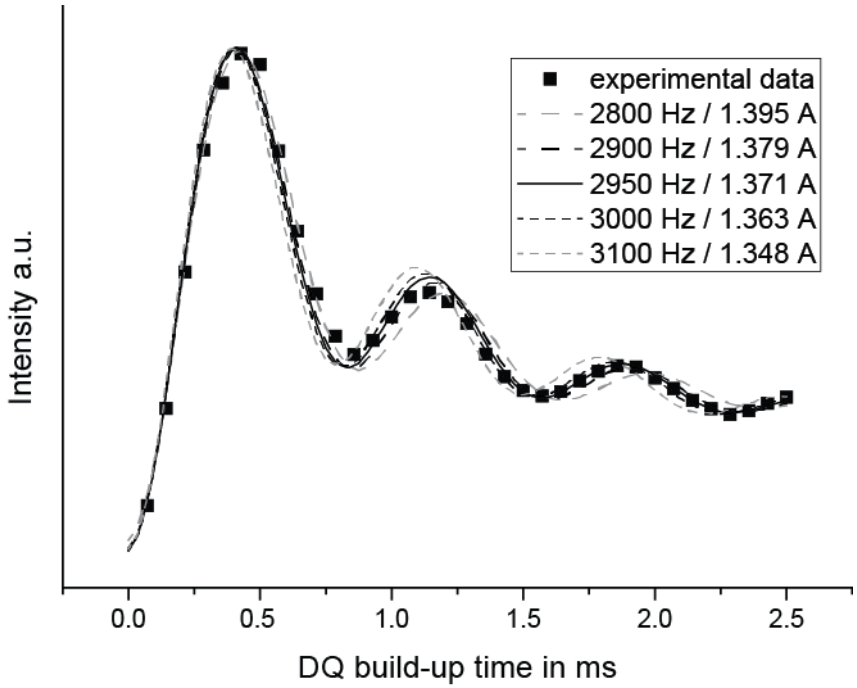

Fig. S7: DQ build-up experiment and SIMPSON simulations for 2,3-$^{13}C_2$-disodium fumarate. Data were recorded under conditions identical to those used for the ChR2 experiments except for microwave irradiation. Due to a very long ^{1}H-T_1, the recycle delay time had to be set to 50 s. The best fit is obtained 2950 ± 150 Hz, which is in good agreement with the expected bond length. An empirical mono-exponential damping function and baseline correction was used to describe the relaxation decay.

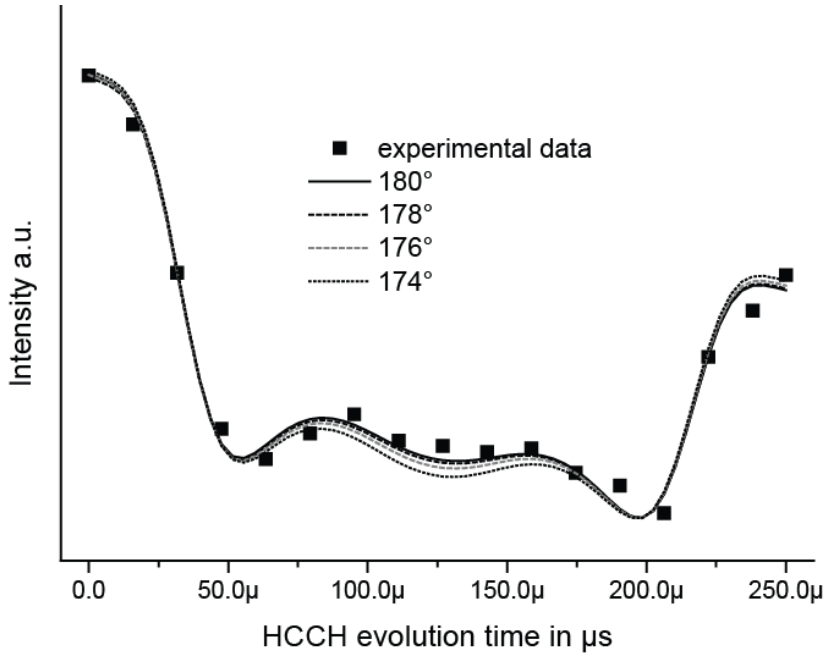

Fig. S8: HCCH dephasing curve for 2,3-$^{13}C_2$-disodium fumarate recorded under conditions identical to those used for the ChR2 experiments except for microwave irradiation. The data agree perfectly well with simulations assuming the expected 180° H-C-C-H torsion angle of this compound.

References

1. Bamann C, Gueta R, Kleinlogel S, Nagel G, & Bamberg E (2010) Structural guidance of the photocycle of channelrhodopsin-2 by an interhelical hydrogen bond. *Biochemistry* 49(2):267-278.
2. Kato HE*, et al.* (2012) Crystal structure of the channelrhodopsin light-gated cation channel. *Nature* 482(7385):369-374.
3. Studier FW (2005) Protein production by auto-induction in high density shaking cultures. *Protein Expr Purif* 41(1):207-234.
4. Mehler M*, et al.* (2013) The EF loop in green proteorhodopsin affects conformation and photocycle dynamics. *Biophys. J.* 105(2):385-397.
5. Sauvee C*, et al.* (2013) Highly efficient, water-soluble polarizing agents for dynamic nuclear polarization at high frequency. *Angew. Chem. Int. Ed. Engl.* 52(41):10858-10861.
6. Fung BM, Khitrin AK, & Ermolaev K (2000) An improved broadband decoupling sequence for liquid crystals and solids. *J. Magn. Reson.* 142(1):97-101.
7. Baldus M, Petkova AT, Herzfeld J, & Griffin RG (1998) Cross polarization in the tilted frame: assignment and spectral simplification in heteronuclear spin systems. *Mol. Phys.* 95(6):1197-1207.
8. Hohwy M, Jakobsen HJ, Edén M, Levitt MH, & Nielsen NC (1998) Broadband dipolar recoupling in the nuclear magnetic resonance of rotating solids: A compensated C7 pulse sequence. *J. Chem. Phys.* 108(7):2686.
9. Concistre M*, et al.* (2012) A large geometric distortion in the first photointermediate of rhodopsin, determined by double-quantum solid-state NMR. *J. Biomol. NMR* 53(3):247-256.
10. Vinogradov E, Madhu PK, & Vega S (1999) High-resolution proton solid-state NMR spectroscopy by phase-modulated Lee-Goldburg experiment. *Chem. Phys. Lett.* 314(5-6):443-450.
11. Mak-Jurkauskas ML*, et al.* (2008) Energy transformations early in the bacteriorhodopsin photocycle revealed by DNP-enhanced solid-state NMR. *Proc. Natl. Acad. Sci. USA* 105(3):883-888.
12. Bak M, Rasmussen JT, & Nielsen NC (2000) SIMPSON: A general simulation program for solid-state NMR spectroscopy. *J. Magn. Reson.* 147(2):296-330.
13. Smith SO*, et al.* (1989) Structure and protein environment of the retinal chromophore in light- and dark-adapted bacteriorhodopsin studied by solid-state NMR. *Biochemistry* 28(22):8897-8904.
14. Carravetta M*, et al.* (2001) Estimation of carbon-carbon bond lengths and medium-range internuclear: Distances by solid-state nuclear magnetic resonance. *J. Am. Chem. Soc.* 123(43):10628-10638.
15. Gupta MP & Sahu RG (1970) The Crystal Structure of Sodium Hydrogen Fumarate. *Acta. Crystallogr. B* B26:1964-1968.
16. Mao J*, et al.* (2014) Structural Basis of the Green–Blue Color Switching in Proteorhodopsin as Determined by NMR Spectroscopy. *J. Am. Chem. Soc.* 136(50):17578-17590.
17. Feng X*, et al.* (2000) Determination of a molecular torsional angle in the metarhodopsin-I photointermediate of rhodopsin by double-quantum solid-state NMR. *J. Biomol. NMR* 16(1):1-8.
18. Nakai T, Ashida J, & Terao T (1989) Influence of small-amplitude motions on two-dimensional N.M.R. powder patterns. *Mol. Phys.* 67(4):839-847.
19. Hamanaka T, Mitsui T, Ashida T, & Kakudo M (1972) The crystal structure of all-trans retinal1. *Acta Crystallogr. Sect. B: Struct. Sci.* 28(1):214-222.
20. Feng X*, et al.* (2000) Determination of a molecular torsional angle in the metarhodopsin-I photointermediate of rhodopsin by double-quantum solid-state NMR. *J. Biomol. NMR* 16(1):1-8.
21. Hosomi H, Ito Y, & Ohba S (1998) Ammonium and Isopropylammonium Salts of the Fumaric Acid Dianion. *Acta Crystallogr. Sect. C-Cryst. Struct. Commun.* 54(1):142-145.

22. Lansing JC*, et al.* (2002) Chromophore distortions in the bacteriorhodopsin photocycle: evolution of the H-C14-C15-H dihedral angle measured by solid-state NMR. *Biochemistry* 41(2):431-438.
23. Feng X*, et al.* (1996) Direct determination of a molecular torsional angle by solid-state NMR. *Chem. Phys. Lett.* 257(3-4):314-320.
24. Bajaj VS, Mak-Jurkauskas ML, Belenky M, Herzfeld J, & Griffin RG (2009) Functional and shunt states of bacteriorhodopsin resolved by 250 GHz dynamic nuclear polarization-enhanced solid-state NMR. *Proc. Natl. Acad. Sci. USA* 106(23):9244-9249.
25. Smith SO, Pardoen JA, Lugtenburg J, & Mathies RA (1987) Vibrational analysis of the 13-cis-retinal chromophore in dark-adapted bacteriorhodopsin. *J. Phys. Chem.* 91(4):804-819.
26. Nack M, Radu I, Bamann C, Bamberg E, & Heberle J (2009) The retinal structure of channelrhodopsin-2 assessed by resonance Raman spectroscopy. *FEBS Lett.* 583(22):3676-3680.
27. Smith SO, Lugtenburg J, & Mathies RA (1985) Determination of retinal chromophore structure in bacteriorhodopsin with resonance Raman spectroscopy. *J. Membr. Biol.* 85(2):95-109.
28. Ames JB*, et al.* (1989) Bacteriorhodopsin's M412 intermediate contains a 13-cis,14-s-trans,15-anti-retinal Schiff base chromophore. *Biochemistry* 28(9):3681-3687.
29. Rodig C, Chizhov I, Weidlich O, & Siebert F (1999) Time-resolved step-scan Fourier transform infrared spectroscopy reveals differences between early and late M intermediates of bacteriorhodopsin. *Biophys. J.* 76(5):2687-2701.
30. Lorenz-Fonfria VA*, et al.* (2013) Transient protonation changes in channelrhodopsin-2 and their relevance to channel gating. *Proc. Natl. Acad. Sci. USA* 110(14):E1273-1281.